AIP | Applied Physics Letters

Elasticity and hardness of nano-polycrystalline boron nitrides: The apparent Hall-Petch effect

A. Nagakubo, H. Ogi, H. Sumiya, and M. Hirao

Citation: Applied Physics Letters **105**, 081906 (2014); doi: 10.1063/1.4894377
View online: http://dx.doi.org/10.1063/1.4894377
View Table of Contents: http://scitation.aip.org/content/aip/journal/apl/105/8?ver=pdfcov
Published by the AIP Publishing

Elasticity and hardness of nano-polycrystalline boron nitrides: The apparent Hall-Petch effect

A. Nagakubo,[1] H. Ogi,[1,a)] H. Sumiya,[2] and M. Hirao[1]
[1]*Graduate School of Engineering Science, Osaka University, Toyonaka, Osaka 560-8531, Japan*
[2]*Advanced Materials R and D Laboratories, Sumitomo Electric Industries, Ltd., Itami, Hyogo 664-0016, Japan*

(Received 23 July 2014; accepted 20 August 2014; published online 27 August 2014)

Nano-polycrystalline boron nitride (BN) is expected to replace diamond as a superhard and superstiff material. Although its hardening was reported, its elasticity remains unclear and the as-measured hardness could be significantly different from the true value due to the elastic recovery. In this study, we measured the longitudinal-wave elastic constant of nano-polycrystalline BNs using picosecond ultrasound spectroscopy and confirmed the elastic softening for small-grain BNs. We also measured Vickers and Knoop hardness for the same specimens and clarified the relationship between hardness and stiffness. The Vickers hardness significantly increased as the grain size decreased, while the Knoop hardness remained nearly unchanged. We attribute the apparent increase in Vickers hardness to the elastic recovery and propose a model to support this insight. © *2014 AIP Publishing LLC*. [http://dx.doi.org/10.1063/1.4894377]

Cubic boron nitride (cBN) is one of important materials for cutting tools because it is superior to diamond in thermal and chemical stability at high temperature. However, its hardness (~50 GPa)[1,2] is smaller than diamond (~100 GPa),[2–4] and many researchers have been attempting to synthesize much harder BN and diamond. One typical method is to be polycrystallized[5–7] and make the grain size d smaller basing of the Hall-Petch effect;[8,9] grain boundaries prevent the dislocation movements, making the material harder. Sumiya and Irifune synthesized nano-polycrystalline diamonds using the direct-conversion method and obtained very hard nano-polycrystalline diamond under an appropriate condition consisting fine grains 10–30 nm in size, whose Knoop hardness H_K exceeded 110 GPa. However, the positive Hall-Petch effect (enhancing hardness with decreasing the grain size) was not clearly observed below it.[7] The direct-conversion methods then succeeded in making the nano-twinned polycrystalline diamonds, which show higher elastic stiffness than monocrystal diamond.[10] Elasticity stiffening brought a great impact because nano-polycrystals often exhibited lower elasticity than monocrystals; grains are weakly bounded, reducing the macroscopic elastic constants.[11–13] Nano-polycrystallization of cBN is therefore expected to achieve the superhard and superstiff material, replacing diamond.

Hardness increases by nano-polycrystallization were reported for BN. Dubrovinskaia *et al*. reported that Vickers hardness H_V consisting of cBN and wurtzite BN (wBN) grains with $d = 14$ nm reached 85 GPa,[14] and Solozhenko *et al*. also reported that nano-cBN synthesized from low-crystallinity pyrolytic hexagonal BN (pBN) at 20 GPa and 1770 K exhibited a high H_V value of 85 GPa,[15] and Tian *et al*. reported that H_V of cBN containing nano-twinned structures exceeded 100 GPa,[16] which is as hard as diamond. However, these values could be overestimated due to the elastic recovery:[17,18] H_V and H_K are widely used for small specimens, but H_K is often smaller than H_V[19–25] and this discrepancy arises from many problems, including friction,[26–28] size effect,[29] crack,[23,30] and elastic recovery.[17–23] Among them, elastic recovery was suggested as the dominant factor and the elastic constant is an important parameter. The unusual stiffening in diamond stems from local twinned (hexagonal diamond) structures.[10] Since fine-grain cBN also contains wBN, which corresponds to a local twinned structure in cBN, it is important to clarify whether the structure stiffening would occur or not for nano-polycrystalline cBN.

Here, we measured the longitudinal-wave elastic constant C_L of different grain size cBNs using picosecond ultrasound spectroscopy, and also measured H_V and H_K of the same specimens to discuss the "real hardness." Indentation tests reflect the mechanical properties only near the surface, and C_L measured by picosecond ultrasound spectroscopy also reflects the elasticity near the surface because the measurable depth is within a few μm for BN. The direct comparison between the elasticity and hardness is thus made possible.

We synthesized 13 nano-polycrystalline cBNs (labeled as BN-1 to BN-13) by the direct-conversion method under high pressure at high temperature from various staring materials of high-purity isotropic hexagonal BN (hBN) compact formed through molding process and three types of pyrolytic hBN (pBN-1, pBN-2, and pBN-3) prepared through CVD-based vapor-phase synthesis. These staring materials were the same as those described in our previous papers.[23,31] The crystallinity levels (degree of graphitization (DOG)) of pBN compacts were in the order of pBN-1 > pBN-2 > pBN-3.[23] To obtain various grain size specimens, we changed starting materials (SMs) and synthesis conditions as synthesis pressure P_s and temperature T_s between 9 and 20 GPa, and 1500 and 2300 °C, respectively, as listed in Table I (more detail synthesis methods appear elsewhere).[23,31] We evaluated the grain size by high resolution scanning electron microscopy.[32]

To measure the elasticity, we developed optics for picosecond ultrasound spectroscopy. We used two titanium/sapphire femtosecond pulse lasers, which are synchronized

a)ogi@me.es.osaka-u.ac.jp

TABLE I. Synthesis condition (SM, DOG, pressure P_s [GPa], and temperature T_s [°C]) of each specimen. Grain size d [nm] is calculated using $T_s - d$ correlation obtained from some SEM images (supplemental Fig. S1).[32] C_L, H_V, and H_K are the measured longitudinal-wave elastic constant, Vickers hardness, and Knoop hardness, respectively, in GPa.

Name	SM	DOG	P_s	T_s	d	C_L	H_V	H_K
BN-13	pBN-3	~0	9	2300	370	957 ± 21	57	43.7
BN-12	hBN	~1	10	2200	300	953 ± 32	…	…
BN-11	hBN	~1	15	2200	300	933 ± 12	…	…
BN-10	hBN	~1	10	2200	300	945 ± 6	…	…
BN-9	pBN-3	~0	9	2100	243	936 ± 10	67	43.6
BN-8	hBN	~1	15	2000	197	928	…	…
BN-7	pBN-3	~0	10	1900	160	920 ± 3	85	45.9
BN-6	pBN-3	~0	20	1900	160	933 ± 3	…	…
BN-5	hBN	~1	15	1800	130	…	…	…
BN-4	pBN-3	~0	20	1700	105	930 ± 3	…	…
BN-3	pBN-3	~0	20	1500	69	922 ± 2	76	46.0
BN-2	pBN-2	0.2	20	1500	69	…	64	44.5
BN-1	pBN-1	0.4	20	1500	69	914 ± 3	77	45.8

within ~100 fs jitter. Their wavelength and repetition rate are 800 nm and 80 MHz, respectively. One laser is used for providing the pump light, which is absorbed in a 10-nm Al thin film deposited on a specimen by the sputtering method and generates an ultrasharp strain pulse through thermal expansion. The other laser provides the time-delayed probe light, whose wavelength is converted into 400 nm by a second-harmonics generator. The probe light pulse is diffracted by the strain pulse backward via the piezo-optic effect and interferes with a reflected probe light from the surface, resulting in a reflectivity oscillation. Details of the optics appear elsewhere.[10] This is called Brillouin oscillation[33,34] and we can observe a specific frequency f component, which satisfies Bragg's condition under normal incidence

$$f = \frac{2nv}{\lambda}, \tag{1}$$

where λ is probe light's wavelength, and n and v are refractive index and sound velocity of a specimen, respectively. We measured n by ellipsometry using instrument M-2000 produced by J. A. Woollam Co.[35] The ellipsometric angles were measured as a function of the wavelength between 370 and 1000 nm, and the Cauchy model was used to inversely determine n. Then, we can obtain v by measuring f. Because the generated strain pulse can be assumed as a longitudinal plane wave, we obtain the longitudinal-wave elastic constant $C_L = \rho v^2$, where ρ is the mass density calculated from lattice constant measured by x-ray diffraction (XRD) in the supplemental material in Fig. S3.[32] XRD spectra show that wBN ratio increased as T_s decreased and that all specimens are composed of cBN and wBN exhibiting no textures or impurities except for BN-9; it includes the remaining hBN less than 2%.

Figure 1(a) shows representative Brillouin oscillations of BN-3 and BN-11. We succeeded in observing Brillouin oscillations except for BN-2 and BN-5; the Brillouin oscillation was not observed in BN-2 and BN-5, and this would be due to the surface condition. We measured at different five points on each specimen and determined C_L using fast Fourier transformation (FFT). Averaged values with their standard deviation (SD) are plotted against d in Fig. 1(c). We found that C_L and its SD decreased with the decrease in d, and here we note that larger SD of larger grain specimens does not indicate experimental error but the elastic-constant variation among different grains. As shown in Figs. 1(a) and 1(b), the measurable region is 3 μm depth from the surface with the 50 μm laser diameter, which contains sufficiently many grains for smaller grain specimens ($d \sim 70$ nm). However, for larger grain specimens, the elastic anisotropy caused by different crystallographic orientations appeared since the largest grain size exceeds a few μm (shown in Fig. S1).[32] This effect is displayed in Fig. 1(b), where C_L of BN-11 exhibits larger fluctuation into depth than that of BN-3. Thus, we succeeded in measuring elasticity only near the surface, where the indentation tests provide the mechanical properties. For the direct comparison between hardness and stiffness, it is important to measure them in the same region and picosecond ultrasound spectroscopy should be used.

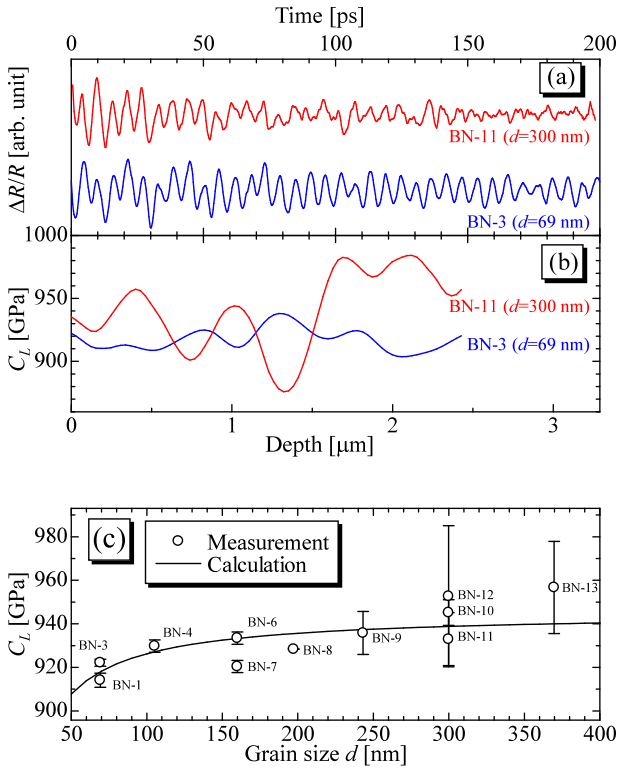

FIG. 1. (a) Observed Brillouin oscillations for BN-3 and BN-11 and (b) corresponding elasticity deviation along depth. We determined local elasticity by applying FFT to Brillouin oscillation in a 50 ps interval. (c) The grain size dependence of C_L. Open circles denote measured C_L and a solid line shows calculated C_L of the composite using micromechanics calculation. Our accurate measurements revealed that C_L and its deviation increased with increase in d.

We attributed the softening in smaller-grain specimens to week inter-grain bounds and estimated their elastic constants using a micromechanics calculation.[36] Actually, larger-grain specimens include more wBNs, and apparent wBN dependence of C_L could be seen. However, we found that the elastic constants of isotropic cBN and wBN are the same in the previous work,[37] insisting that wBN content dependence does not have to be considered. Then, we considered our specimens as composites, including softened penny-shaped inclusions of cBN, simulating grain boundaries, and

the matrix of pure cBN, whose elastic constants $\mathbf{C}_M$ were determined in the previous work.[37] The elastic stiffness tensor $\mathbf{C}_C$ of the composite can be calculated by Eshelby's equivalent inclusion theory using Mori-Tanaka mean field modeling[38,39]

$$\mathbf{C}_C = \mathbf{C}_M + V_f(\mathbf{C}_I - \mathbf{C}_M)\mathbf{A}, \tag{2}$$

$$\mathbf{A} = \mathbf{A}_D[(1 - V_f)\mathbf{I} + V_f\mathbf{A}_D]^{-1}, \tag{3}$$

$$\mathbf{A}_D = [\mathbf{I} + \mathbf{S}\mathbf{C}_M^{-1}(\mathbf{C}_I - \mathbf{C}_M)]^{-1}. \tag{4}$$

Here, $\mathbf{C}_I$ and V_f denote the elastic stiffness tensor and volume fraction of inclusions, respectively, $\mathbf{S}$ is the Eshelby tensor, and symbol $\mathbf{I}$ is the unit matrix. We assumed that the aspect ratios α and V_f of the inclusion are written as functions of grain size d and the grain-boundary thickness t as $V_f = \frac{2t}{\sqrt{3}d}$ and $\alpha = \frac{t}{d}$ assuming the 2D honeycomb structure (see the supplemental material).[32] We inversely determined $\mathbf{C}_I$ using the least squares method to fit the calculated C_L^C to the measured C_L. Because grain-boundary thicknesses of nano-polycrystalline BNs in high-resolution transmission electron microscopy images were about a few nm,[16] we calculated for $t = 3a$, $6a$, and $10a$, where a is the lattice constant ($a = 3.6182$ Å). We assumed that the bulk modulus B^I of inclusions is constant and only the share modulus G^I decreases: in the previous work, we found that the grain boundaries of the nano-polycrystalline diamond have lower resistance to shear deformation and proposed graphitic inclusions,[40] which were experimentally confirmed.[41] The nano-polycrystalline BN would have similar structures, leading to significantly lower shear stiffness at grain boundaries.

We show obtained elastic constants in Fig. 2. Calculated C_L^C shows a good agreement with measured C_L for all t values, and we find that G^I should be significantly smaller (by $55 \sim 86\%$). Fine-grain specimens were synthesized from nano-hBN particles at relatively low T_s to prevent the crystal growth, and it is likely that their grain boundaries have not been converted to cBN completely. The out-of-plane shear modulus of hBN (C_{44}) is significantly small,[42] corresponding to low shear modulus at the grain boundaries.

Finally, we discuss the relationship between the elasticity and hardness. Figure 3 shows measured H_V and H_K as plotted for C_L. Importantly, there is an enormous discrepancy between H_V and H_K at smaller d values. H_V greatly increases (up to 50%) as d decreases, while H_K increases by a few percents, indicating that Hall-Petch effect would make the nano-polycrystalline BN slightly harder. Large differences between H_K and H_V (more than 30%) stem from some reasons. One reason is cracks; many cracks are observed for Vickers indentation, leading to a variation of indentation shape and unclear edges.[23] The larger error bars of H_V in Fig. 3 will be caused by this effect. Another important reason is the elastic recovery and we attribute the increase in H_V to the elastic recovery: $H_K = \beta_K \frac{P}{L^2}$ is calculated only from the longer diagonal L of the indentation, whose elastic recovery can be neglected comparing with the shorter diagonal w.[17] (β_K is the shape factor for the Knoop indenter and P is the load.) On the other hand, in the Vickers indentation, the two diagonals length D equivalently become shorter on the unloading process, leading to overestimation of $H_V = \beta_V \frac{P}{D^2}$, where β_V is the shape factor for the Vickers indenter.[18] In fact, many researchers have reported that H_K is smaller than H_V. Gong *et al.*[19] and Chicot *et al.*[21] found a linear correlation between H_V/H_K and w/L, which represents elastic recovery in the Knoop indentation,[17] and Ullner *et al.* proposed corrected hardness by estimating depth recovery on unloading.[20] However, there is no research that measured the elasticity and hardness for the same materials of different hardness.

To quantitatively discuss the recovery effect, we calculated strain-stress fields of an elliptical hole under uniformly stressed plate, and deduced the displacements along the longer and shorter diagonals of the elliptical hole u_L and u_w as follows:[43]

$$u_L = \frac{2p}{E}w = \frac{2p}{E}\frac{L}{\gamma}, \tag{5}$$

$$u_w = \frac{2p}{E}L = \frac{2p}{E}\gamma w, \tag{6}$$

where p is the uniform stress, E is Young's modulus, and γ is the ratio L/w which equals to 7.11 and 1 for the Knoop and

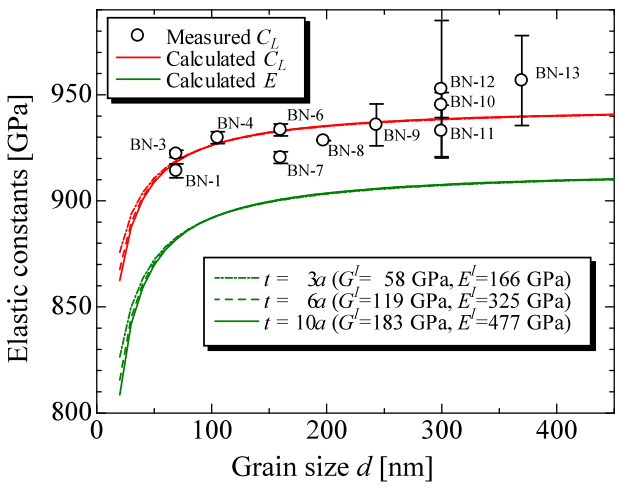

FIG. 2. Calculated C_L and Young's modulus E of composite for (solid line) $t = 10a \approx 3.6$ nm, (dashed line) $t = 6a \approx 2.2$ nm, (chain line) $t = 3a \approx 1.1$ nm, where a is lattice constant. G^I and E^I are the shear and Young's moduli of inclusions for each t, respectively. Calculated C_L shows a good agreement with measured value (open circles and red lines). E is used for the discussion in the elastic recovery.

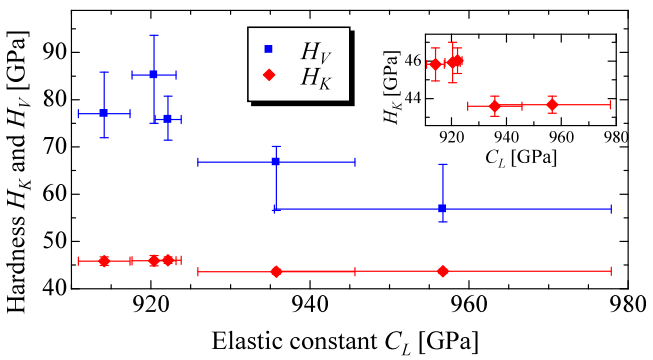

FIG. 3. Knoop hardness H_K and Vickers hardness H_V plotted for longitudinal-wave elastic constant C_L. H_V was larger than H_K and largely increased as C_L decreased, while H_K increased only by 2%, indicating elastic recovery leads to overestimation of H_V.

Vickers indenter, respectively. This elastic recovery occurs on unloading and leads to overestimation of the hardness. The recovered hardness H'_V and H'_K is written as

$$H'_V = \beta_V \frac{P}{(D-u_D)^2} = \frac{H_V}{(1-2p/E)^2}, \quad (7)$$

$$H'_K = \beta_K \frac{P}{(L-u_L)^2} = \frac{H_K}{(1-2p/\gamma E)^2}, \quad (8)$$

where u_D denotes the recovered displacement of the diagonal of the circle, simulating the Vickers indenter. Note that H_V and H_K are essentially the same ($H_V = H_K = H_0$) and p is comparable with the hardness value because the stress around an indenter can be calculated from the same equation of the hardness. Then, we calculated H'_V and H'_K for $H_0 = p = 42$ GPa and $200 < E < 1000$ GPa as shown in Fig. 4. H'_V is larger than H_0 by more than 20% and significantly increases with the decrease in E; on the other hand, H'_K is much less sensitive to E, insisting that Vickers hardness can be largely overestimated by the elastic recovery, while the Knoop hardness is less affected. If E of polycrystalline cBN changes between 200 and 600 GPa, the elastic recovery can quantitatively explain the difference between measured H_V and H_K values. Our measurement and micromechanics calculation results indicate that the grain boundary sliding would play an important role in the indentation: E of pure cBN is 915 GPa and it macroscopically decreases by 5% at most ($E \approx 870$ GPa). From the micromechanics calculations, the elasticity of grain boundary should be much smaller than that of the macroscopic composite values; their Young's modulus is about 300 GPa for $t = 6a$ nm (Fig. 2). These softened regions will be fairly deformed and its volume fraction increases with the decrease in d. As a result, considerable elastic deformation occurs within the grain boundaries in a small-grain specimen, which leads to significant overestimation of H_V, and it increases as the elasticity decreases with decrease in d, exhibiting an apparent Hall-Petch effect.

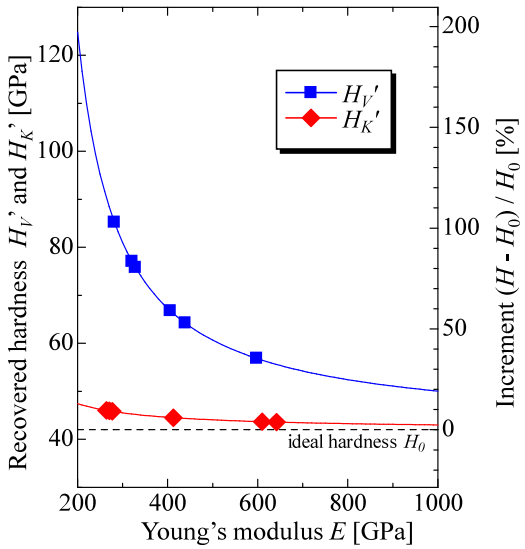

FIG. 4. Blue and red lines represent the recovered hardness calculated from Eqs. (7) and (8) for $p = H_0 = 42$ GPa, respectively, and solid symbols denote the measured hardness plotted on the lines. H_V is incorrectly overestimated by more than 20% and exhibits an apparent Hall-Petch effect.

In summary, we measured the C_L of 13 nano-polycrystalline cBN specimens, and found that elasticity of nano-polycrystalline cBN decreased as d decreased due to the increment of the softened grain boundaries, whose elastic constants were estimated to be $14 \sim 45\%$ of pure cBN from micromechanics calculations. These softened grain boundaries lead to significant overestimation of H_V of BNs; while measured H_K was nearly independent from d and C_L, H_V increased by 50% at most. We considered that elastic recoveries caused these considerable difference and deduced elastically recovered hardness H'_V and H'_K. The increment of H'_V exceeds 100% and exhibits an apparent Hall-Petch effect: H'_V increases with decrease in E. H_K is much less sensitive to elastic recovery, insisting that we should use H_K for superhard materials.

[1]C. A. Brookes, R. M. Hooper, and W. A. Lambert, Philos. Mag. A **47**, L9 (1983).
[2]C. A. Brookes, *The Properties of Diamond*, edited by J. E. Field (Academic Press, London, 1979).
[3]C. A. Brookes, Nature **228**, 660 (1970).
[4]H. Sumiya, N. Toda, and S. Satoh, Diamond Relat. Mater. **6**, 1841 (1997).
[5]M. Akaishi, T. Satho, M. Ihsii, T. Taniguchi, and S. Yamaoka, J. Mater. Sci. Lett. **12**, 1883 (1993).
[6]T. Taniguchi, M. Akaishi, and S. Yamaoka, J. Am. Ceram. Soc. **79**, 547 (1996).
[7]H. Sumiya and T. Irifune, J. Mater. Res. **22**, 2345 (2007).
[8]E. O. Hall, Proc. Phys. Soc. B **64**, 747 (1951).
[9]N. J. Petch, J. Iron Steel Inst. **174**, 25 (1953).
[10]K. Tanigaki, H. Ogi, H. Sumiya, K. Kusakabe, N. Nakamura, M. Hirao, and H. Ledbetter, Nat. Commun. **4**, 2343 (2013).
[11]G. W. Nieman and J. R. Weertman, J. Mater. Res. **6**, 1012 (1991).
[12]T. Y. Zhang and J. E. Hack, Phys. Status Solidi A **131**, 437 (1992).
[13]E. Bonetti, E. G. Campari, L. D. Bianco, and G. Scipione, Nanostruct. Mater. **6**, 639 (1995).
[14]N. Dubrovinskaia, V. L. Solozhenko, N. Miyajima, V. Dmitriev, O. O. Kurakevych, and L. Dubrovinsky, Appl. Phys. Lett. **90**, 101912 (2007).
[15]V. L. Solozhenko, O. O. Kurakevych, and Y. L. Godec, Adv. Mater. **24**, 1540 (2012).
[16]Y. Tian, B. Xu, D. Yu, Y. Ma, Y. Wang, Y. Jiang, W. Hu, C. Tang, Y. Gao, K. Luo, Z. Zhao, L. M. Wang, B. Wen, J. He, and Z. Liu, Nature **493**, 385 (2013).
[17]D. B. Marshall, T. Noma, and A. G. Evans, J. Am. Ceram. Soc. **65**, C175 (1982).
[18]B. R. Lawn and V. R. Howes, J. Mater. Sci. **16**, 2745 (1981).
[19]J. Gong, J. Wang, and Z. Guan, Mater. Lett. **56**, 941 (2002).
[20]C. Ullner, J. Beckmann, and R. Morrell, J. Eur. Ceram. Soc. **22**, 1183 (2002).
[21]D. Chicot, D. Mercier, F. Roudet, K. Silva, M. H. Staia, and J. Lesage, J. Eur. Ceram. Soc. **27**, 1905 (2007).
[22]H. S. Guder, E. Sahin, O. Sahin, H. Gocmez, C. Duran, and H. A. Cetinkara, Acta Phys. Pol. A **120**, 1026 (2011), http://przyrbwn.icm.edu.pl/APP/SPIS/a120-6.html.
[23]H. Sumiya, Y. Ishida, K. Arimoto, and K. Harano, Diamond Relat. Mater. **48**, 47 (2014).
[24]C. A. Brookes and B. Moxley, J. Phys. E **8**, 456 (1975).
[25]R. S. Lima, A. Kucuk, and C. C. Berndt, Surf. Coat. Technol. **135**, 166 (2001).
[26]M. Atkinson and H. Shi, Mater. Sci. Technol. **5**, 613 (1989).
[27]C. Shaw, Y. Li, and H. Jones, Mater. Lett. **28**, 33 (1996).
[28]H. Shi and M. Atkinson, J. Mater. Sci. **25**, 2111 (1990).
[29]M. Atkinson, J. Mater. Sci. **30**, 1728 (1995).
[30]P. Feltham and R. Banerjee, J. Mater. Sci. **27**, 1626 (1992).
[31]H. Sumiya, K. Harano, and Y. Ishida, Diamond Relat. Mater. **41**, 14 (2014).

[32]See supplementary material at http://dx.doi.org/10.1063/1.4894377 for detail procedures of calculating grain sizes and volume fraction of grain boundaries.
[33]A. Devos and R. Cote, Phys. Rev. B **70**, 125208 (2004).
[34]H. Ogi, T. Shagawa, N. Nakamura, M. Hirao, H. Odaka, and N. Kihara, Phys. Rev. B **78**, 134204 (2008).
[35]H. G. Tompkins and W. A. McGahan, *Spectroscopic Ellipsometry and Reflectometry* (Wiley, New York, 1999).
[36]H. Ogi, G. Shimoike, M. Hirao, K. Takashima, and Y. Higo, J. Appl. Phys. **91**, 4857 (2002).
[37]A. Nagakubo, H. Ogi, H. Sumiya, K. Kusakabe, and M. Hirao, Appl. Phys. Lett. **102**, 241909 (2013).
[38]T. Mura, *Micromechanics of Defects in Solids*, 2nd ed. (Martinus Nijhoff, The Hague, 1987).
[39]T. Mori and K. Tanaka, Acta Metall. **21**, 571 (1973).
[40]H. Ogi, N. Nakamura, H. Tanei, M. Hirao, R. Ikeda, and M. Takemoto, Appl. Phys. Lett. **86**, 231904 (2005).
[41]H. F. Cheng, H. Y. Chiang, C. C. Horng, H. C. Chen, C. S. Wang, and I. N. Lin, J. Appl. Phys. **109**, 033711 (2011).
[42]L. Duclaux, B. Nysten, J. P. Issi, and A. W. Moore, Phys. Rev. B **46**, 3362 (1992).
[43]S. P. Timoshenko and J. N. Goodier, *Theory of Elasticity*, 3rd ed. (McGraw-Hill, New York, 1970).